PHYSICAL AND ELECTROMAGNETIC PROPERTIES OF Tm AND Gd SUBSTITUTED Mg-Mn FERRITES

NILAR LWIN

UNIVERSITI SAINS MALAYSIA

2013

PHYSICAL AND ELECTROMAGNETIC PROPERTIES OF Tm AND Gd SUBSTITUTED Mg-Mn FERRITES

by

NILAR LWIN

Thesis submitted in fulfilment of the

requirements for the degree of

Doctor of Philosophy

April 2013

ACKNOWLEDGEMENTS

I would like to express my sincere gratitude and heartfelt thanks to my main supervisor, Professor Dr. Ahmad Fauzi Mohd Noor for inspiring guidance, constructive criticism and valuable suggestions till the completion of this work at Universiti Sains Malaysia, USM. It would have not been possible for me to bring out this thesis without his help and constant encouragement. I wish that he will keep in touch with me in future and will continue to give his valuable advice.

I also would like to thanks to my co-supervisors, Professor Dr. Radzali Othman and Assoc Prof Dr. Srimala Sreekantan for their constructive comments, invaluable suggestions and guidance at various stages of the work. I am also grateful to Assoc Prof Dr Widad Ismail, School of Electrical and Electronic Engineering, USM for her useful suggestions and help whenever I had asked for it to carry out my research work.

I wish to express my special gratitude to my sister Assoc Prof Dr Aye Aye Thant, Physics Department, University of Yangon for helping me a lot to conduct my higher studies in USM.

It is a pleasant duty to acknowledge Dean, Deputy Dean, all lecturers, administrative and technical staffs in the School of Materials and Mineral Resources Engineering, USM for their continual supports and assistance to finish this work. I wish to give them my special thanks for their constant help.

I would like to convey my sincere thanks to all of my teachers starting from Primary School until now. Their nourishment facilitated me to reach this height. My special thanks to all my friends in USM, for their great companion and help making my stay in Malaysia pleasant and enjoyable. All activities that we had together are unforgettable. Their friendship is a blessing, my heart will always treasure. I am thanking my best friend Dr Pradip Kumar Roy, India for his encouragements. I wish to record my thanks and gratitude to him for his valuable suggestions and patient to answer all my questions whenever I asked throughout my study.

I am grateful to Universiti Sains Malaysia for providing me a 3 years scholarship to conduct this research. Also I sincerely thanks to e-Science Fund" (Grant No. 6013343), the Ministry of Science, Technology and Environment-MOSTI (03-01-05-SF 0375) for financial support in this work.

Finally, I would like to take this opportunity to express my heartfelt thanks to my beloved parents; U Own Maung and Daw Own Win who have been instrumental in raising me up to the height that I am in at present with their love, courage and support. This thesis is dedicated to them. My special appreciation and gratitude goes to my aunty Daw Kyi Aye, my sister, my brother and sister in law for their love and kindness.

Thank you.
Nilar Lwin
April 2013

TABLE OF CONTENTS

Page

ACKNOWLEDGEMENTS……..……..ii

TABLE OF CONTENTS…….....iv

LIST OF TABLES…….……..……x

LIST OF FIGURES…….xiii

LIST OF ABBREVIATIONS……..…xx

LIST OF PUBLICATIONS…….……xxiv

ABSTRAK…….……xxvi

ABSTRACT…….xxviii

CHAPTER 1: INTRODUCTION

1.1 Background of research 1

1.2 Problem statement..... 4

1.3 Objectives of research..... 6

1.4 Approach to research 7

1.5 Organization of thesis 8

CHAPTER 2: LITERATURE REVIEW

2.1 Introduction..... 10

2.2 Crystal structure of ferrite..... 10

2.3 Crystal structure of orthoferrite 15

2.4 Magnetic properties 16

2.4.1 Basic concepts 16

2.4.1.1 Magnetic Field and Dipoles 16

2.4.1.2 Origin of Magnetic moments 16

2.4.1.3 Magnetic behavior..... 18

2.4.1.4 Magnetic domain 20
2.4.1.5 Metal ions distribution over octahedral and tetrahedral sites 23
2.4.1.6 Magnetic interactions in ferrites 24
2.4.1.7 Magnetization curve and hysteresis loops 25
2.5 Electrical properties 28
2.5.1 Frequency dependent electrical properties 28
2.6 Effect of divalent cation substitution 35
2.7 Effect of iron deficient in ferrite 39
2.8 Effect of rare earth cation substitution 40
2.9 Synthesis method of Mg and Mg-Mn ferrites 45
2.10 Applications of ferrite 52
2.10.1 Microstrip patch antenna application of ferrite 54
2.11 Summary of review 56

CHAPTER 3: MATERIALS AND METHODOLOGY

3.1 Introduction 58
3.2 Starting materials 59
3.3 Design of experiment 60
3.4 Synthesis of Ferrite Powder by Citrate Precursor Method 60
3.4.1 $MgFe_2O_4$ ferrite Synthesized by CPM 60
3.4.2 Composition formulation 63
3.4.3 Calcination 64
3.4.4 De-agglomeration 64
3.5 Synthesis of Ferrite Powder by Solution Combustion 65
3.5.1 $MgFe_2O_4$ and $Mg_{0.9}Mn_{0.1}Fe_{2-x}O_4$ Synthesized by SC 65
3.5.2 Composition Formulation 66
3.5.3 Calcination 69

3.5.4 De-agglomeration 69
3.6 Fabrication and sintering of ferrite parts 70
3.6.1 Fabrication 70
3.6.2 Sintering 71
3.7 Characterization techniques of powder and sintered specimens 72
3.7.1 Thermal Analysis (TG/DTA) 72
3.7.2 Dilatometry 73
3.7.3 X-ray Diffraction (XRD) 74
3.7.4 Field Emission Scanning Electron Microscopy (FESEM) 76
3.7.5 Transmission Electron Microscopy (TEM) 77
3.7.6 Density and Porosity Measurement 78
3.7.7 Magnetization Properties Measurement 80
3.7.8 Electrical Properties Measurement 81
3.8 Design of rectangular microstrip patch antenna printed on Mg-Mn ferrite 84
3.8.1 Simulation of microstrip patch antenna on Mg-Mn ferrite substrate 86
3.8.2 RF sputtering of Copper deposition on Mg-Mn ferrite substrate 87
3.9 S- parameter measurement 88
3.10 Antenna radiation pattern measurement 89

CHAPTER 4: RESULTS AND DISCUSSION91

4.1 Introduction 91
4.2 Optimization of synthesis method 91
4.2.1 Synthesis of $MgFe_2O_4$ ferrite by Citrate Precursor Method (CPM) 91
4.2.2 TG/DTA – Thermal Analysis 92
4.2.3 Phase Formation 93
4.2.4 TEM microstructural analysis 95
4.2.5 Optimization of sintering temperature 95

4.2.6 Phase Formation of sintered pellet 96

4.2.7 Densification and microstructural observation 98

4.2.8 Evaluation of magnetic properties..... 101

4.2.9 Evaluation of electrical properties..... 105

4.3 Synthesis of $MgFe_2O_4$ ferrite by Solution Combustion Method (SCM) 110

4.3.1 TG/DTA – Thermal Analysis of the precursor 110

4.3.2 XRD – Phase formation 112

4.3.3 TEM microstructural analysis 115

4.3.4 Densification and microstructural observation of sintered samples..... 116

4.3.5 Evaluation of magnetic properties..... 118

4.3.6 Evaluation of electrical properties..... 121

4.3.7 Summary 124

4.4 Effect of Fe deficient Mg-Mn ferrite ($Mg_{0.9}Mn_{0.1}Fe_{2-x}O_4$) synthesized by SCM 126

4.4.1 Introduction 126

4.4.2 TG/DTA – Thermal Analysis of the precursor 126

4.4.3 Phase formation of as burnt powder and sintered specimens..... 127

4.4.4 TEM microstructural analysis 130

4.4.5 Densification and microstructural observation 131

4.4.6 Evaluation of magnetic properties..... 137

4.4.7 Evaluation of electrical properties..... 139

4.4.8 Summary 143

4.5 Effect of Tm substitution on Fe deficient Mg-Mn ferrite ($Mg_{0.9}Mn_{0.1}Fe_{2-x}Tm_xO_4$) synthesized by SCM 144

4.5.1 Introduction 144

4.5.2 Phase formation..... 144

4.5.3 TEM microstructural analysis 148

4.5.4 Densification and microstructural observation 149

4.5.5 Evaluation of magnetic properties 154

4.5.6 Evaluation of electrical properties 157

4.5.7 Summary 161

4.6 Effect of Gd substitution on Fe deficient Mg-Mn ferrite ($Mg_{0.9}Mn_{0.1}Fe_{2-x}Gd_xO_4$) synthesized by SCM 162

4.6.1 Introduction 162

4.6.2 Phase formation 162

4.6.3 TEM microstructural analysis 166

4.6.4 Densification and microstructural observation 167

4.6.5 Evaluation of magnetic properties 171

4.6.6 Evaluation of electrical properties 174

4.6.7 Summary 179

4.7 Antenna application of the product 180

4.7.1 Rectangular patch antenna measurement 181

4.7.2 Bandwidth determination 184

4.7.3 Radiation pattern determination 186

CHAPTER 5: CONCLUSION AND FUTURE WORK

5.1 Conclusions 190

5.2 Future work 192

REFERENCES

APPENDIX A 206

APPENDIX B 207

APPENDIX C 208

APPENDIX D 212

APPENDIX E 213

APPENDIX F 215

APPENDIX G 218

LIST OF TABLES

		Page
Table 2.1:	Radii of Metal ions involved in Spinel ferrite	12
Table 2.2:	Metal ion distribution in ferrites	14
Table 2.3:	Bohr magneton of ions commonly found in magnetic materials	18
Table 2.4:	Summary of review on the effect of different rare earth cation substitutions in ferrite	44
Table 2.5:	Summary of review on the synthesis methods of Mg and Mg-Mn ferrites	51
Table 3.1:	Physical properties of starting materials to synthesize by CPM and SCM	59
Table 3.2:	Weight of the starting materials to prepare $MgFe_2O_4$ ferrite in citrate precursor method	63
Table 3.3:	Weight of the starting materials to prepare $MgFe_2O_4$ and $Mg_{0.9}Mn_{0.1}Fe_{2-x}O_4$ ferrite in solution combustion method	66
Table 3.4:	Weight of the starting materials to prepare Tm substituted $Mg_{0.9}Mn_{0.1}\,Tm_xFe_{1.8-x}O_4$ in solution combustion method	68
Table 3.5:	Weight of the starting materials to prepare Gd substituted $Mg_{0.9}Mn_{0.1}\,Gd_xFe_{1.8-x}O_4$ in solution combustion method	68
Table 3.6:	Parameters of the Mg-Mn ferrite patch antenna substrate and grown plane	86
Table 3.7:	Parameters being set in equipment for Cu deposition	88
Table 4.1:	Lattice parameter and X-ray density of $MgFe_2O_4$ ferrite by CPM	98
Table 4.2:	Bulk density, relative density and porosity of $MgFe_2O_4$ ferrites by CPM	99
Table 4.3:	Total porosity, open porosity and closed porosity of $MgFe_2O_4$ ferrites by CPM	100
Table 4.4:	The value of M_s, M_r, H_c and n_B for the $MgFe_2O_4$ ferrites with different sintering temperature prepared by CPM	103

Table 4.5:	Expected cation distribution in $MgFe_2O_4$ ferrite by CPM sintered at different temperature	105
Table 4.6:	Resistivity of $MgFe_2O_4$ ferrite prepared by CPM for the different sintering temperature	110
Table 4.7:	Crystallite size, lattice parameter and X-ray density of $MgFe_2O_4$ ferrite by SCM	115
Table 4.8:	Bulk density, relative density and porosity of $MgFe_2O_4$ ferrites by SCM	117
Table 4.9:	The value of M_s, M_r, H_c and n_B for the $MgFe_2O_4$ ferrites prepared by SCM with different sintered temperature	119
Table 4.10:	Expected cation distribution in $MgFe_2O_4$ ferrite by SCM sintered at different temperature	121
Table 4.11:	Resistivity of $MgFe_2O_4$ ferrites prepared by SCM for the different sintering temperature	124
Table 4.12:	Crystallite size, lattice parameter and X-ray density of $Mg_{0.9}Mn_{0.1}Fe_{2-x}O_4$ ferrite by SCM	130
Table 4.13:	Bulk density, relative density and porosity of $Mg_{0.9}Mn_{0.1}Fe_{2-x}O_4$ ferrites by SCM	134
Table 4.14:	The value of M_s, M_r, H_c and n_B for the $Mg_{0.9}Mn_{0.1}Fe_{2-x}O_4$ ferrites with different Fe content prepared by SCM	137
Table 4.15:	Expected cation distribution in $Mg_{0.9}Mn_{0.1}Fe_{2-x}O_4$ ferrites with different Fe content prepared by SCM	138
Table 4.16:	Resistivity of $Mg_{0.9}Mn_{0.1}Fe_{2-x}O_4$ ferrite prepared by SCM with different Fe content	142
Table 4.17:	Bulk density, relative density and porosity of $Mg_{0.9}Mn_{0.1}Tm_xFe_{1.8-x}O_4$ ferrites by SCM	152
Table 4.18:	The value of M_s, M_r, H_c and n_B for the $Mg_{0.9}Mn_{0.1}Tm_xFe_{2-x}O_4$ ferrites prepared by SCM with different Tm content	156
Table 4.19:	Expected cation distribution in $Mg_{0.9}Mn_{0.1}Tm_xFe_{1.8-x}O_4$ ferrites prepared by SCM with different Tm content	157
Table 4.20:	Resistivity of $Mg_{0.9}Mn_{0.1}Tm_xFe_{1.8-x}O_4$ ferrite prepared by SCM for the different Tm content	161

Table 4.21:	Lattice parameter of sintered $Mg_{0.9}Mn_{0.1}Gd_xFe_{1.8-x}O_4$ ferrite (1250^oC) with different compositions	164
Table 4.22:	Bulk density, relative density and porosity of $Mg_{0.9}Mn_{0.1}Gd_xFe_{1.8-x}O_4$ ferrites by SCM	167
Table 4.23:	The value of M_s, M_r, H_c and n_B for the $Mg_{0.9}Mn_{0.1}Gd_xFe_{1.8-x}O_4$ ferrites prepared by SCM with different Fe content	174
Table 4.24:	Expected cation distribution in $Mg_{0.9}Mn_{0.1}Gd_xFe_{1.8-x}O_4$ ferrites prepared by SCM with different Fe content	174
Table 4.25:	Dielectric constant of $Mg_{0.9}Mn_{0.1}Gd_xFe_{1.8-x}O_4$ and $Mg_{0.9}Mn_{0.1}Tm_xFe_{1.8-x}O_4$ ferrite sintered at 1250^oC for different compositions measured at frequency 1MHz	175
Table 4.26:	Resistivity of $Mg_{0.9}Mn_{0.1}Gd_xFe_{1.8-x}O_4$ ferrite prepared by SCM sintered at 1250^oC for the different Gd content	179
Table 4.27:	Comparison between dielectric constant, resistivity and magnetization of Mg-Mn ferrite with different composition	181
Table 4.28:	Comparison between patch antenna printed on Mg-Mn ferrite to others	186

LIST OF FIGURES

		Page
Figure 2.1:	Two sub cells of a unit cell of the spinel structure	11
Figure 2.2:	A perovskite structure of an orthoferrite	15
Figure 2.3:	Demonstration of the magnetic moment associated with (a) an orbiting electron and (b) a spinning electron	17
Figure 2.4:	Different types of magnetic behaviour [Mathew, 2007]	19
Figure 2.5:	Schematic depiction of domains in a ferromagnetic or ferrimagnetic material	21
Figure 2.6:	Illustration of domain and domain wall	21
Figure 2.7:	Division into domains	22
Figure 2.8:	Interionic distances and angles in the spinel structure for the different type of lattice sites interactions. [Smit and Wijin, 1959]	25
Figure 2.9:	Magnetization curve with domain configurations at different stages of magnetization [Kittel, 1956]	26
Figure 2.10:	Initial magnetization curve and hysteresis loop [Sellymer and Skomaski, 2006]	28
Figure 2.11:	Schematic representation of different mechanism of polarization (Hippel, 1954)	30
Figure 2.12:	Dispersion in dielectric constant and resistivity for a nickel-zinc ferrite (Koops, 1951)	32
Figure 2.13:	Capacitor with a double layer dielectric	33
Figure 2.14:	Equivalent circuits of double layer dielectric	33
Figure 2.15:	Differential thermal analysis (DTA) and thermo-gravimetry (TG) curves of as-prepared $MgFe_2O_4$ powders [Hirota, K. et al. 2008]	48
Figure 2.16:	TG and DSC curves of the as-synthesized MgFe2O4 precursor [Huang et al., 2006]	50
Figure 2.17:	Classifications of ferrites	52

		Page
Figure 2.18:	Wide range of applications of ferrites [Bahadur, 1992]	53
Figure 2.19:	Standard patch antenna with microstrip feed on a substrate	55
Figure 2.20:	(a) Rectangular microstrip patch antenna, (b) Circular microstrip patch antenna, and (c) Triangular microstrip patch antenna [Saxena et al., 2009]	56
Figure 3.1:	Flow chart of overall view of experiments	61
Figure 3.2:	Schematic flow chart of the synthetic pathway of Mg ferrite from citrate precursor method	62
Figure 3.3:	Heating profile of the calcination process in CPM	64
Figure 3.4:	Schematic presentation of powder preparation technique for the pure phase Mg-Mn Ferrite	67
Figure 3.5:	A flow chart of fabrication and characterization of sintered ferrite parts	70
Figure 3.6:	A typical sintering profile of ferrite specimens	72
Figure 3.7:	Position of pellets during sintering process	72
Figure 3.8:	A simple vibrating sample magnetometer (VSM)	81
Figure 3.9:	HP/Agilent 4291B RF impedance/material analyser	82
Figure 3.10:	Physical and effective length of rectangular microstrip patch	85
Figure 3.11:	Simulation of microstrip patch antenna on Mg-Mn ferrite substrate (a) Simulation (b) experimental	87
Figure 3.12:	RF sputtering CVD system	88
Figure 3.13:	Hewlett Packard Network Analyzer (Agilent Technology E8364B, 10MHz to 50GHz)	89
Figure 3.14:	The equipment set up for microstrip patch antenna on Mg-Mn ferrite substrate radiation patterns measurement.	90

		Page
Figure 4.1:	TG & DTA plots for as prepared powder for $MgFe_2O_4$	93
Figure 4.2:	XRD spectrum for as prepared powder of $MgFe_2O_4$ ferrite	94
Figure 4.3:	XRD spectrum of $MgFe_2O_4$ ferrite powder calcined at 500^oC (● = $MgFe_2O_4$)	94
Figure 4.4:	TEM micrograph of $MgFe_2O_4$ ferrite powder calcined at 500^oC by CPM	95
Figure 4.5:	The densification and temperature curve for the compact powder	96
Figure 4.6:	XRD of $MgFe_2O_4$ ferrite powder sintered at different temperature (a) 1100^oC, (b) 1150^oC, (c) 1200^oC and (d) 1250^oC prepared by CPM (• = $MgFe_2O_4$)	97
Figure 4.7:	Variation of density and porosity on the different sintering temperatures of $MgFe_2O_4$ ferrites prepared by CPM	98
Figure 4.8:	SEM micrographs of fracture surface for $MgFe_2O_4$ ferrite sintered at (a) 1100^oC, (b) 1150^oC, (c) 1200^oC, (d) 1250^oC	101
Figure 4.9:	The magnetization curves of $MgFe_2O_4$ ferrites with different sintered temperature measured by VSM ±10kOe at room temperature	102
Figure 4.10:	Variation of dielectric constant with sintering temperature for $MgFe_2O_4$ ferrite	106
Figure 4.11:	Variation of loss tangent with frequency for $MgFe_2O_4$ ferrite sintered at different temperature	108
Figure 4.12:	Variation of resistivity with frequency for $MgFe_2O_4$ ferrite sintered at different temperature	109
Figure 4.13:	TG and DTA plots of the precursor for $MgFe_2O_4$ ferrite	112
Figure 4.14:	XRD spectra of (a) as-burnt powders (b) calcined powder (500^oC)	114
Figure 4.15:	XRD spectra of $MgFe_2O_4$ ferrites prepared by SCM sintered at (a) 1100^oC (b) 1150^oC, (c) 1200^oC, (d) 1250^oC	114
Figure 4.16:	TEM micrograph of $MgFe_2O_4$ ferrite powder calcined at 500^oC by SCM	116

		Page
Figure 4.17:	Variation of density and porosity on the different sintering temperatures of $MgFe_2O_4$ ferrite prepared by SCM.	117
Figure 4.18:	SEM micrographs of $MgFe_2O_4$ ferrites prepared by SCM sintered at (a) 1100^oC, (b) 1150^oC, (c) 1200^oC, (d) 1250^oC	118
Figure 4.19:	The magnetization curves of $MgFe_2O_4$ ferrites prepared by SCM with different sintering temperature measured by VSM ±10kOe at room temperature	120
Figure 4.20:	Variation of dielectric constant with different sintering temperature for $MgFe_2O_4$ ferrite prepared by SCM	122
Figure 4.21:	Variation of loss tangent with frequency for $MgFe_2O_4$ ferrite prepared by SCM sintered at different temperature	123
Figure 4.22:	Variation of resistivity with frequency for $MgFe_2O_4$ ferrite prepared by SCM sintered at different temperature	123
Figure 4.23:	TG and DTA plots of the precursor for $Mg_{0.9}Mn_{0.1}Fe_{1.8}O_4$ ferrite	127
Figure 4.24:	XRD spectra of as-burnt powders for (a) x=0.2, (b) x=0.4, (c) x=0.6, (d) x=0.8	128
Figure 4.25:	XRD spectra of calcined powders for (a) x=0.2, (b) x=0.4, (c) x=0.6, (d) x=0.8	129
Figure 4.26:	XRD spectra of sintered pellets at 1250$^oC$for (a) x=0.2, (b) x=0.4, (c) x=0.6, (d) x=0.8	130
Figure 4.27:	TEM micrographs of calcined powders at 500^oC for $Mg_{0.9}Mn_{0.1}Fe_{2-x}O_4$ ferrite (a) x=0.2, (b) x=0.4, (c) x=0.6 and (d) x=0.8	131
Figure 4.28:	Variation of density and porosity on the different composition of Mg-Mn ferrites	132
Figure 4.29:	SEM micrographs of the fractured surface of $Mg_{0.9}Mn_{0.1}Fe_{2-x}O_4$ ferrite (a) x=0.2, (b) 0.4, (c) x=0.6, (d) x=0.8 sintered at 1250°C	133
Figure 4.30:	EDX analysis of $Mg_{0.9}Mn_{0.1}Fe_{2-x}O_4$ ferrites sintered at 1250^oC by SCM (a) x=0.2, (b) x=0.4, (c) x=0.6 and (d) x=0.8 (Inset is the compositional ratio of the elements)	135

Figure 4.31:	The magnetization curves of $Mg_{0.9}Mn_{0.1}Fe_{2-x}O_4$ ferrites with different Fe content measured by VSM ±10kOe at room temperature	138
Figure 4.32:	Variation of dielectric constant with composition for $Mg_{0.9}Mn_{0.1}Fe_{2-x}O_4$ ferrites sintered at 1250^oC for different samples	140
Figure 4.33:	Variation of Loss tangent with frequency for $Mg_{0.9}Mn_{0.1}Fe_{2-x}O_4$ ferrite sintered at 1250^oC for different samples	141
Figure 4.34:	Variation of resistivity with frequency for $Mg_{0.9}Mn_{0.1}Fe_{2-x}O_4$ ferrite sintered at 1250^oC	143
Figure 4.35:	XRD spectra of $Mg_{0.9}Mn_{0.1}Fe_{2-x}Tm_xO_4$ ferrite as burnt powder of (a) x=0.0, (b) x= 0.025 (c) x = 0.050, (d) x=0.075	145
Figure 4.36:	XRD spectra of $Mg_{0.9}Mn_{0.1}Fe_{2-x}Tm_xO_4$ ferrite calcined powder (500^oC) of (a) x=0.0, (b) x= 0.025 (c) x = 0.050, (d) x=0.075	145
Figure 4.37:	XRD spectra of $Mg_{0.9}Mn_{0.1}Fe_{2-x}Tm_xO_4$ ferrite sintered pellets (1250^oC) of (a) x = 0.0, (b) x = 0.025, (c) x = 0.05, (d) x = 0.075	147
Figure 4.38:	XRD patterns of $Mg_{0.9}Mn_{0.1}Fe_{1.8-x}Tm_xO_4$ ferrites with x = 0.025 in each (a) as burnt powder (b) calcined powder and (c) sintered pellets	148
Figure 4.39:	TEM images of $Mg_{0.9}Mn_{0.1}Tm_xFe_{1.8-x}O_4$ ferrite (a) x=0.0 (b) x=0.025, (c) x=0.050 and (d) x=0.075	149
Figure 4.40:	Variation of density and porosity of sintered $Mg_{0.9}Mn_{0.1}Fe_{1.8-x}Tm_xO_4$ ferrites with different Tm content (x=0.0, 0.025, 0.050, 0.075)	150
Figure 4.41:	SEM images of $Mg_{0.9}Mn_{0.1}Tm_xFe_{1.8-x}O_4$ ferrite (a) x=0.0 (b) x=0.025, (c) x=0.050 and (d) x=0.075	151
Figure 4.42:	EDX analysis of $Mg_{0.9}Mn_{0.1}$ $Tm_xFe_{1.8-x}O_4$ pellets sintered at 1250^oC by SCM (a) x=0.0 (b) x=0.025 (c) x=0.050 (d) x=0.075	152

Figure 4.43:	The magnetization curves of $Mg_{0.9}Mn_{0.1}Tm_xFe_{1.8-x}O_4$ ferrites measured by VSM ±10kOe at room temperature	155
Figure 4.44:	Variation of dielectric constant with composition for $Mg_{0.9}Mn_{0.1}Tm_xFe_{1.8-x}O_4$ ferrite sintered at 1250^oC	158
Figure 4.45:	Variation of Loss tangent with frequency for $Mg_{0.9}Mn_{0.1}Tm_xFe_{1.8-x}O_4$ ferrite sintered at 1250^oC	159
Figure 4.46:	Variation of resistivity with frequency for $Mg_{0.9}Mn_{0.1}Tm_xFe_{1.8-x}O_4$ ferrite sintered at 1250^oC	160
Figure 4.47:	XRD spectra of $Mg_{0.9}Mn_{0.1}Gd_xFe_{1.8-x}O_4$ ferrite as burnt powder of (a) x=0.0, (b) x= 0.025, (c) x = 0.050, (d) x=0.075	164
Figure 4.48:	XRD spectra of $Mg_{0.9}Mn_{0.1}Gd_xFe_{1.8-x}O_4$ ferrite calcined powders (500^oC) of (a) x=0.0, (b) x= 0.025, (c) x = 0.050, (d) x=0.075	165
Figure 4.49:	XRD spectra of $Mg_{0.9}Mn_{0.1}Gd_xFe_{1.8-x}O_4$ ferrite sintered pellets (1250^oC) of (a) x=0.0, (b) x= 0.025, (c) x = 0.050, (d) x=0.075	165
Figure 4.50:	TEM images of $Mg_{0.9}Mn_{0.1}Gd_xFe_{1.8-x}O_4$ ferrite (a) x= 0.0 (b) x=0.025, (c) x=0.050 and (d) x=0.075	166
Figure 4.51:	Variation of density and porosity of sintered $Mg_{0.9}Mn_{0.1}Gd_xFe_{1.8-x}O_4$ ferrites with different Gd content (x=0.0, 0.025, 0.050, 0.075)	167
Figure 4.52:	SEM images of $Mg_{0.9}Mn_{0.1}Gd_xFe_{1.8-x}O_4$ ferrite (a) x= 0.0 (b) x=0.025, (c) x=0.050 and (d) x=0.075	168
Figure 4.53:	EDX analysis of $Mg_{0.9}Mn_{0.1}Gd_xFe_{1.8-x}O_4$ pellet sintered at 1250^oC by SCM (a) x=0.025 (b) x=0.050 (c) x=0.075	170
Figure 4.54:	The magnetization curves of $Mg_{0.9}Mn_{0.1}Gd_xFe_{1.8-x}O_4$ ferrites with different compositions measured by VSM ±10kOe at room temperature	173
Figure 4.55:	Variation of dielectric constant with composition for $Mg_{0.9}Mn_{0.1}Gd_xFe_{1.8-x}O_4$ ferrite sintered at 1250^oC	176
Figure 4.56:	Variation of loss tangent with frequency for $Mg_{0.9}Mn_{0.1}$ $Gd_xFe_{1.8-x}O_4$ ferrite sintered at 1250^oC	177

Figure 4.57:	Variation of resistivity with frequency for $Mg_{0.9}Mn_{0.1}Gd_xFe_{1.8-x}O_4$ ferrite sintered at 1250^oC	179
Figure 4.58:	Return loss and frequency measurement of patch antenna printed on Mg-Mn ferrite substrate	182
Figure 4.59:	Input impedance of the microstrip patch antenna from 5 to 20 GHz	184
Figure 4.60:	Bandwidth (%BW) measurement [Jasik, 1984]	185
Figure 4.61:	Radiation pattern of microstrip patch antenna printed on Mg-Mn ferrite for (a) E-plane and (b) H-plane	188
Figure 4.62:	3D simulation radiation pattern for far field application	189

LIST OF ABBREVIATIONS

°C	: Degree Centigrade
Å	: Angstrom
a	: Lattice Parameter
AC	: Alternating current
Al	: Aluminum
approx.	: Approximately
$BaFe_{12}O_{19}$	: Barium Ferrite
$C_6H_8O_7.H_2O$	: Citric Acid
CPM	: Citrate Precursor Method
CST	: Computer Simulation Technology
Cd	: Cadmium
CO_2	: Carbon Dioxide
Co^{2+}	: Cobalt (2+) ion
$CoFe_2O_4$	: Cobalt ferrite
Cp	: Parallel Capacitance
Cr^{3+}	: Chromium
Cu	: Copper
Cu^{2+}	: Copper (2+) ion
D	: Dissipation Factor
DC	: Direct current
DTA	: Differential Thermal Analysis
Dy	: Dysprosium
EDS	: Energy Dispersive Spectroscopy
EDX	: Energy Dispersive X-Ray
EMI	: Electromagnetic Interference
Er	: Erbium
Eu	: Europium
fcc	: Face Centered Cubic
Fe	: Iron
$Fe(NO_3)_3.9H_2O$	: Iron Ntrate
Fe^{2+}	: Ferrous ion

Fe_2O_3	: Iron Oxide
Fe^{3+}	: Ferric ion
FEG	: Field Emission Gun
FWHM	: Full Width at Half Maximum
g	: gram
g/mol	: gram per mole
Gd	: Gadolinium
GHz	: Gigahertz
H	: Magnetic Field
H_2O	: Water
H_c	: Coerceivity
Ho	: Holmium
HRTEM	: High resolution transmission electron microscope
K	: Kelvin
kg m^{-3}	: kilogram per cubic meter
kJ/g	: kilojoule per gram
kOe	: Kilooersted
kV	: Kilovolt
LC	: Inductance-Capacitance
LCR	: Inductance Capacitance Resistance
M	: Molarity
Mg	: Magnesium
$Mg(NO_3)_2.6H_2O$	: Magnesium Nitrate
Mg^{2+}	: Magnesium (2+) ion
$MgFe_2O_4$	: Magnesium Ferrite
MgO	: Magnesium Oxide
M-H	: Magnetization versus Hysteresis curve
MHz	: Megahertz
ml	: milliliter
ml/min	: Milliliter per minute
mm	: Millimeter
MMIC	: Monolithic Microwave Integrated Circuits
Mn	: Manganese ion
$Mn(NO_3)_2.6H_2O$	: Magnese Nitrate

Mn^{2+} : Manganese (2+) ion

$MnFe_2O_4$: Manganese Ferrite

MnO : Manganese Oxide

MPa : Megapascal

M_r : Remanent Magnetization

M_s : Satuation Magnetization

N_2 : Nitrogen

nA : nanoampere

n_B : Magnetic moment per unit cell (magneton number)

NH_4NO_3 : Ammonium Nitrate

Ni^{2+} : Nickel (2+) ion

$NiFe_2O_4$: Nickel Ferrite

Ni-Zn : Nickel-Zinc

nm : nanometer

NO_2 : Nitrogen Dioxide

NO^{3-} : Nitrate

O_2 : Oxygen

Rp : Parallel Resistance

rpm : revolution per minute

SEM : Scanning Electron Microscope

SCM : Solution Combustion Method

SiC : Silicon Carbide

SiO_2 : Silicon Dioxide

Sm : Samarium

tan δ : Loss tangent

Tb : Terbium

T_c : Curie Temperature

TEM : Tranmission Electron Microscope

TG : Thermal Gravimetry

TG-DTA : Thermogravimetry- Differential Thermal Analysis

Ti : Titanium

Tm : Thulium

T_N : Neel Temperature

VSM : Vibrating Sample magnetometer

XPS	: X-ray Photoelectron Spectrometer
XRD	: X-ray Diffraction
Y	: Yttrium
Zn^{2+}	: Zinc (2+) ion
$ZnFe_2O_4$	: Zinc ferrite
μ_B	: Bohr magneton
μm	: Micrometer
Ωm	: Ohm meter

LIST OF PUBLICATIONS

1. Nilar Lwin, Ahmad Fauzi M.N, Srimala Sreekantan, Radzali Othman, Aye Aye Thant (2011) "Physical properties characterization of Fe-deficient $Mg_{0.9}Mn_{0.1}Fe_{2-x}O_4$ soft ferrite by citrate precursor method" *Journal of Materials Science and Engineering, USA, Vol 5, No.8, p 506-511, ISSN: 1934-8959.*

2. Nilar Lwin, Ahmad Fauzi M.N, Srimala Sreekantan, Radzali Othman, Aye Aye Thant (2011) "Effect of Fe deficiency on structural and magnetic properties in low temperature synthesized Mg-Mn ferrite" *International journal of nanoscience, Vol 10, No.6,* DOI No: 10.1142/S0219581X11008393, *ISSN: 0219-581x.*

3. Nilar Lwin, Ahmad Fauzi M.N, Srimala Sreekantan, Radzali Othman, Aye Aye Thant (2013) "A novel and simple process for nanosized Mg-Mn ferrite preparation from solution combustion method and study of its characteristics" International journal of Applied Ceramic Technology, (Accepted) ISSN: 1744-7402.

4. Nilar Lwin, Aye Aye Thant, Srimala Sreekantan, Radzali Othman and Ahmad Fauzi M. N. (2010) Low-temperature processing of nanosized Mg-Mn ferrite and some of its characteristics. *Malaysian Journal of Microscopy, 6(1), p.91-95.*

5. Nilar Lwin, Aye Aye Thant, Srimala Sreekantan, Radzali Othman and Ahmad Fauzi M. N. (2010) Effect of iron deficient on physical and dielectric properties changes of magnesium-manganese soft ferrite system. *Malaysian Journal of Microscopy, 7(1), p.127-131.*

6. Nilar Lwin, Aye Aye Thant, Srimala Sreekantan, Radzali Othman and Ahmad Fauzi M. N. (2009) Synthesis and Characterization of $MgFe_2O_4$ ferrite by Citrate Precursor Method. *4th International Conference on Recent Advances in Materials, Minerals & Environment and 2nd Asian Symposium on Materials & Processing, Penang Malaysia.* 1st-3rd June 2009. Penang, Malaysia.

7. Nilar Lwin, Aye Aye Thant, Srimala Sreekantan, Radzali Othman and Ahmad Fauzi M. N. (2009) Formation and characterization of $MgFe_2O_4$ soft ferrite prepared via citrate precursor route. *The Symposium of USM fellowship holders 2009.* 14th-15th November 2009. Universiti Sains Malaysia, Malaysia.

8. Nilar Lwin, Aye Aye Thant, Srimala Sreekantan, Radzali Othman and Ahmad Fauzi M. N. (2009) Low-temperature processing of nanosized Mg-Mn ferrite and some of its characteristics. *The 18th Scientific Conference Electron Microscopy Society of Malaysia & 19th Annual General Meeting of EMSM.* 15th-17th December 2009. Kula Lumpur, Malaysia.

9. Nilar Lwin, Ahmad Fauzi M.N, Srimala Sreekantan, Radzali Othman, Aye Aye Thant (2010) "Physical properties characterization of Fe-deficient $Mg_{0.9}Mn_{0.1}Fe_{2-x}O_4$ soft ferrite by citrate precursor method" Proceedings of 7th International Materials Technology Conference and Exhibition. Kuching, Sarawak.

10. Nilar Lwin, Aye Aye Thant, Srimala Sreekantan, Radzali Othman and Ahmad Fauzi M. N. (2010) Effect of iron deficient on physical and dielectric properties changes of magnesium-manganese soft ferrite system. *The 19th Scientific Conference Electron Microscopy Society of Malaysia & 20th Annual General Meeting of EMSM.* 14th-16th December 2010. Langkawi, Malaysia. (Best Poster Award).

11. Nilar Lwin, Aye Aye Thant, Srimala Sreekantan, Radzali Othman and Ahmad Fauzi M. N. (2011) Effect of sintering temperature on physical and electromagnetic properties of $MgFe_2O_4$ ferrites via solution combustion method. The 20th Scientific Conference Electron Microscopy Society of Malaysia & 21th Annual General Meeting of EMSM. 20th-22th December 2011. Permasuri Resort, Port Dickson, Negeri Sembilan, Malaysia.

12. Nilar Lwin, Ahmad Fauzi M.N, Srimala Sreekantan, Radzali Othman, Aye Aye Thant (2011) "Synthesis and characterization of Magnesium ferrite by solution combustion method" Proceedings of 1st International Conference on Materials Engineering and 3rd AUN/SEED-Net Regional Conference on Materials Engineering (RCME) 2010, Jogyakata, Indonesia.

13. Nilar Lwin, Aye Aye Thant, Srimala Sreekantan, Radzali Othman and Ahmad Fauzi M. N. (2012) Synthesis and characterization of Gd substituted Mg-Mn ferrite by solution combustion method. The 21th Scientific Conference Electron Microscopy Society of Malaysia & 22th Annual General Meeting of EMSM. 22th-24th November 2012. Renaissance Hotel, Kota Bharu Kelantan, Malaysia.

SIFAT FIZIK DAN ELEKTROMAGNET FERIT Mg-Mn DITUKARGANTI DENGAN Tm DAN Gd

ABSTRAK

Dalam kajian ini, magnesium ferit telah dihasilkan menerusi dua kaedah, iaitu kaedah bahan mula sitrat (CPM) dan kaedah pembakaran larutan (SCM). Serbuk yang terhasil daripada kedua-dua kaedah telah dikaji dari sudut struktur, morfologi dan sifat elektromagnet. Menerusi kaedah CPM, fasa tunggal ferit $MgFe_2O_4$ yang bersaiz nano (10-15 nm) telah dihasilkan pada suhu 500°C, dan ini dikenalpasti daripada analisa XRD ke atas serbuk sintesis. Sebaliknya kaedah SCM turut menghasilkan fasa tunggal ferit yang bersaiz nano lebih halus (8-9 nm) pada suhu yang lebih rendah, iaitu sekitar 200°C. Ekoran ini kaedah SCM telah dipilih untuk menghasilkan ferit $Mg_{0.9}Mn_{0.1}Fe_{2-x}O_4$ dengan komposisi x=0.2, 0.4, 0.6 dan 0.8 untuk menentukan kesan kandungan Fe yang berbeza. Analisis XRD mengesahkan kesemua spesimen mempamerkan kehadiran fasa spinel kubik. Dari segi sifat, kerintangan diperhatikan meningkat bila kandungan Fe semakin mengurang. Komposisi $Mg_{0.9}M_{n0.1}Fe_{1.8}O_{0.4}$ telah didpati mempamerkan ketumpatan tertinggi 4.26g/cm^3, pemalar dielektrik (11.136), kerintangan tinggi dan pemagnetan tepu tertinggi (38.41 emu/g). Seterusnya dengan menggunakan komposisi ini sebagai asas, penukargantian Tm telah dilakukan dan ini didapati menghasilkan fasa kedua $TmFeO_3$. Begitu juga sifat-sifat fizik dan elektromagnet telah berubah dengan kandungan Tm. Ketumpatan pukal didapati menurun daripada 4.26 kepada 3.82 g/cm^3 dengan meningkatnya kepekatan Tm. Dari sudut sifat magnet, didapati pemagnetan tepu telah menurun dengan meningkatnya penggantian Tm. Kerintangan

tertinggi ($39.84x10^6$ Ω-cm) telah diperhatikan pada komposisi $Mg_{0.9}Mn_{0.1}F_{e1.725}Tm_{0.075}O_4$. Selain penukargantian Tm, kesan penukargantian Gd ke atas struktur dan sifat electromagnet ferit Mg-Mn turut dikaji. Penukargantian Gd telah memudahkan pembentukan fasa kedua pada sempadan butir. Peningkatan kandungan Gd telah menyebabkan ketumpatan pukal ferit tersinter menurun, sebaliknya kerintangan elektrik meningkat. Ferit dengan pemalar dielektrik rendah dalam julat 6-12 telah diperhatikan dan tiada maksimum kehilangan dielektrik dalam tempoh masa frekuensi yang diukur sehingga 1GHz. Secara umum, ferit Mg-Mn dengan sifat elektromagnet yang boleh direka khusus telah dicadangkan untuk menghasilkan lapisan mikro antena tampal. Untuk tujuan ini, beberapa parameter penting untuk antena tampal telah dianalisis seperti kehilangan balik, jalur lebar dan corak sinaran. Keselarian telah berjaya diperolehi di antara keputusan simulasi dan eksperimen. Antena ini telah didapati berfungsi dengan baik dalam frekuensi 15 dan 18 GHz. Justeru itu, Mg-Mn ferrit boleh digunakan sebagai substrat antena pelbagai jalur.

PHYSICAL AND ELECTROMAGNETIC PROPERTIES OF Tm AND Gd SUBSTITUTED Mg-Mn FERRITES

ABSTRACT

In this work, magnesium ferrite was firstly fabricated by citrate precursor method (CPM) and solution combustion method (SCM). The structural, morphological, and electromagnetic magnetic properties of the ferrites from both methods were investigated. Using CPM, a single phase and nano-sized (10-15 nm) $MgFe_2O_4$ ferrite was formed at 500^oC as evidenced from XRD analysis of the synthesized powders. On the other hand, SCM had produced single phase ferrite with nanosize of (8-9 nm) at around 200^oC. Subsequently, SCM was chosen to produce $Mg_{0.9}Mn_{0.1}Fe_{2-x}O_4$ with x=0.2, 0.4, 0.6 and 0.8 to determine the effect of varying Fe content. The XRD analysis confirms that all the specimens showed the presence of cubic spinel phase. In terms of properties, the resistivity was observed to increase when Fe content were reduced. The $Mg_{0.9}Mn_{0.1}Fe_{2-x}O_4$ was found to show highest density (4.26 g/cm^3), dielectric constant (11.136), higher resistivity, and a high saturation magnetization (38.41 emu/g). Then, using this compostion as the base, Tm substitution was performed and this was found to produce a secondary phase $TmFeO_3$. It was also found that the physical and magnetic properties had changed with Tm content. Bulk density was found to decrease from 4.26 to 3.82 g/cm^3 with increasing Tm. From the magnetic properties, it was found that saturation magnetization had decreased with increase of Tm. Highest resistivity (39.84 x 106 Ω-cm) was observed for $Mg_{0.9}Mn_{0.1}Fe_{1.725}Tm_{0.075}O_4$. Besides Tm substitution, the effect of Gd substitution on structural and electromagnetic properties of ferrite was also investigated. The substitution of Gd had easily formed secondary phase at grain boundaries. Increase in

Gd had resulted in lowering of the bulk density of ferrite, but increase in electrical resistivity. Ferrite with a low dielectric constant in the range of 6-12 was observed and there was no maximum dielectric loss in the frequency range measured to 1 GHz. Generally, Mg-Mn ferrite with electromagnetic properties that can be tailored was proposed for patch layer microstrip antenna. For this purpose, several parameters for this patch antenna were analysed, such as return loss, bandwidth and radiation pattern. Good compatibility was obtained between the simulation and experimental results. The antenna was found to work successfully in the frequency range of 15 and 18 GHz. Hence, the Mg-Mn ferrite was found to be able to use as multiband antenna substrate.

CHAPTER 1

INTRODUCTION

1.1 Background of research

Ferrite ceramics are magnetic materials, dark gray or black in appearance and contain iron oxide as a major constituent in it [Moulson and Herbert, 2003]. Based on the crystal structure, ferrites have been categorized as spinels, perovskites, garnets and hexaferrites. They can also be classified as soft, hard, microwave and square loop depending on their magnetic performance [Patil et al., 2008]. Nowadays, ferrites are used as essential parts in most electric and electronic equipments and devices. In the new materials area, ferrites with permeabilities of 20,000 and 30,000 have been made available commercially. Moreover, power ferrites which have been made available for frequencies up to 10 MHz [Viswanathan & Murhty, 1990]. With improvements and innovations continue to take place, many new applications, theories and preparation technologies are exploited in the field of ferrites.

Ferrites are known commercially important materials as a result of their excellent electrical and magnetic properties such as low dielectric constant, low dielectric losses, high resistivity, low coercivity and low saturation magnetization etc. The electrical and magnetic properties of ferrites are strongly dependent on the purity of the starting ferrite powder, the microstructure as well as the grain boundary chemistry. Typically, high purity, uniform composition and developing good microstructure are essential for high performance of the ferrites [He et al., 2005]. Generally, adding small amount of additives or improving process and firing program could enhance the properties of the ferrites.

There are many types of ferrites in magnetic materials, such as magnesium ferrite, zinc ferrite, nickel ferrite, nickel-copper-zinc ferrite etc [Paik et al., 2005, Seyyed Ebrahimi and Azadmanjiri, 2007]. Magnesium ferrite, $MgFe_2O_4$, is a soft magnetic material with a spinel structure and it is being used in many applications like heterogeneous catalysis, adsorption, and sensors and in magnetic technologies [Pradhan et al., 2005]. The magnesium ferrites are ferrimagnetic oxides with permanent magnetization, called ferrimagnetism. The unit cell is based on closed-packed oxygen lattice with the interstitial position being filled by metallic ions and these ions occupy two sites: tetrahedral (A) sites, where each metallic ion is surrounded by four oxygen ions and the octahedral (B) sites, where each metallic ion is surrounded by six oxygen ions [Bueno et al., 2007].

Among the different ferrites, Mg-Mn ferrites are considered as the most versatile ferrites due to their high resistivity at carrier frequency, low losses (10^{-2} to 10^{-3}) for high frequency and they can be employed in microwave applications [Pandit et al., 2005]. The properties of ferrites are known to be sensitive to changes in the different compositions, which in turn affect the cation distribution over the tetrahedral A site and the octahedral B site. The addition of divalent and trivalent ions in ferrites influences the electrical and magnetic properties of the system [Chhaya and Kulkarni, 2000]. Hence, in order to understand the magnetic properties of spinel ferrites, the knowledge of cation distribution and spin arrangement is essential.

There are ample literatures available on the study of Mg ferrite and Mn substituted Mg ferrite. Mansour and Elkestawy, [2011] reported their work on Mg

ions replacing Mn ions in $MnFe_2O_4$ keeping the amount of Fe constant and investigated the effect of Mg substitution on the structural, electrical and magnetic properties. They found that X-ray diffraction analysis for both nanosize and bulk samples revealed the nanocrystalline nature in the prepared ferrite samples. The crystallite sizes were in the range of 3-6 nm for nano powders and 63-85.9 nm for bulk samples sintered at 1200^oC. The dielectric constant values of this study are ten orders of magnitudes. The low dielectric behavior makes ferrite materials useful in high frequency applications. However, information on the effect of Fe deficiency on the electrical and magnetic properties in Mg-Mn ferrite is scarce. Iron deficiency plays an important role in the physical, electrical and magnetic properties of the ferrite materials such as phase formation, density-porosity, dielectric constant, dielectric loss, resistivity and saturation magnetization [Zhiyuan et al., 2000]. Hence, it is necessary to study the physical and electromagnetic properties as a function of Fe deficiency in Mg-Mn ferrites.

Besides that, additives and selection of materials are influenced on the properties of ferrites. Several investigators reported the influence of rare earth on the properties of different ferrites required for high frequency applications. Magnetic behavior of the ferromagnetic oxides is largely governed by the Fe-Fe interaction (the spin coupling of the 3d electrons) and introducing rare earth ions into the spinel lattice, the Rare earth (R)-Fe interaction also appear (3d-4f coupling). This would lead to changes in both electrical and magnetic properties of the ferrite [Zhao et al., 2005].

1.2 Problem statement

In the preparation of electromagnetic ferrite materials, particular attentions are generally given to the purity of the raw materials, stoichiometry of the composition and the porosity as well as grain characteristics of the final product. As the properties and performance of ferrites are sensitive to their composition and microstructure, which in turn depend upon the technique involved to synthesize them, the selection and choice of the process adopted is the key to obtain high quality ferrites. Most ferrites have been produced by the conventional process involving high temperature solid-state reaction between the constituent oxides. There are some inherent drawbacks using this process such as formation of undesirable phases, non-homogeneous grain sizes due to firing at high temperature and poor chemical homogeneity [Kumar et al., 2009]. In addition, milling of raw material can introduce chemical impurities into the final product, thus affecting the ferrite properties.

Therefore, attempts toward improving the technological performance of ferrites have led to the development of various wet chemical methods which have been reported for the production of homogeneous, fine and reproducible ferrites [Verma et al., 2006, Mathew et al., 2007, Li and Wang, 2009, Mansour et al., 2011]. However, low production rate and complex schedules are the common problems associated with chemical methods. Optimization of synthesis of the wet chemical methods such as sol-gel, co-precipitation, microemulsion, citrate precursor, hydrothermal, solution combustion, is very important to produce improved ferrites with reduce energy consumption and low production cost.

On the other hand, there are also some problems in patch antenna applications. The microstrip patch antennas using FR-4 and Duroid substrate with very low dielectric constant can have some operational limitations such as restricted bandwidth of operation, low gain and low radiation efficiency due to surface wave losses [Gonzalo and Nagore, 2002]. Moreover, high signal loss in large size antenna results in poor antenna performance at high frequency applications. Therefore it is necessary to solve these problems in order to improve the properties of substrate materials which could be used for high performance patch antenna applications.

In recent years, as a result of the need for the high frequency applications, the use of magnetic materials had increased. Ferrite is one of the important magnetic materials which are used in mono and polycrystalline form. Some novel characteristics of polycrystalline ferrite such as low dielectric constant, low dielectric losses, and high resistivity over normal dielectric material make it very useful in microwave antenna applications. The reason for using ferrite materials in microstrip structures is that the applied magnetic field changes the permeability of the magnetic materials and thus electrical properties, which in turn changes the antenna properties. This would result in the antenna size to be reduced considerably with the reduction of surface wave excitation and loss [Saxena et al., 2009]. In fact, it could be approached to tune the electromagnetic properties of ferrite by synthesis method, compositions of compounds and heat treatment on the materials.

The microstrip antenna has been widely used in achieving the objective of maximal integration for personal communication devices. The advantages of microstrip patch antenna are reported to be low profile, ease of fabrication using

printed circuit techniques resulting in low cost and also easy integration with microwave integrated circuits [Balanis, 1997]. Hence, the integration of ferrite technology into microstrip patch antenna has numerous advantages and potential applications. To date, no literatures are available reporting the study of microstrip patch antenna printed on Mg-Mn ferrite substrate and the knowledge on antenna performance has not yet received study.

Taking this background into consideration, this research work was embarked upon to prepare and characterized $MgFe_2O_4$ ferrite by the citrate precursor method (CPM) and solution combustion method (SCM) to provide good understanding on the behavior of ferrite and the changes caused by the synthesis methods on structural, electrical and magnetic properties. After optimizing the synthesis method based on the properties obtained, the second stage was the preparation of Fe deficient and rare earth substituted Mg-Mn ferrites nanocrystallites by solution combustion method. The physical and electromagnetic properties of Mn and rare earth substitution in Fe deficient Mg ferrites were explored. Finally, this ferrite product was applied to use as microstrip patch antenna and the antenna performance was investigated.

1.3 Objectives of research

The principal objectives of this present research are:

(1) To optimize synthesis methods (CPM and SCM) to produce $MgFe_2O_4$ ferrites with tailored properties.

(2) To investigate effect of Fe deficient on the structural, electrical and magnetic properties of Mg-Mn ferrite.

(3) To study effect of Tm^{3+} and Gd^{3+} substitution in Fe^{3+} on the structural and electromagnetic properties of Mg-Mn ferrites.

(4) To fabricate microstrip patch antenna and investigate the antenna performance (impedance bandwidth, return loss, and radiation pattern).

1.4 Approach to research

To achieve the above mention objectives, this research was conducted to optimize the synthesis method to produce $MgFe_2O_4$ ferrites in this work. Citrate Precursor Method (CPM) and Solution Combustion Method (SCM) were employed for the synthesis of $MgFe_2O_4$ ferrites in this study. Upon completion of synthesis method optimization, the effect of Fe deficient on the electromagnetic properties of Mg-Mn ferrites was investigated. Subsequently, the effects of rare earth elements Tm and Gd substitutions on electromagnetic properties of Mg-Mn ferrites were discussed in details. Lastly, the microstrip patch antenna was fabricated by using Mg-Mn ferrite as a substrate material and investigated the antenna performance which can be used for high frequency applications.

Hence, a systematic study regarding the formation of Mg and Mg-Mn ferrites is performed and the materials are characterized with respect to phase formation, microstructure and electromagnetic properties. In addition to that, a complete set of data regarding the measurements of antenna performance of microstrip patch antenna using a new substrate material (Mg-Mn ferrite) is presented for this research.

1.5 Organization of thesis

This thesis has been divided into five chapters:

Chapter one starts with brief introduction of Mg and Mg-Mn ferrites based on magnetic materials for antenna application. The primary objectives and the general flow of the whole research program are also carefully outlined as well as organize the thesis overview.

Chapter two deals with detail literature review. Attempts have been made to systematically classify the available information under different sections. This chapter incorporates background information to assist in understanding the aims and objectives of this investigation, and also reviews recent reports by other investigators with which these results can be compared.

Chapter three presents the brief explanation of the physical properties of starting materials, i.e magnesium nitrate, maganese nitrate, iron nitrate, thulium nitrate, gadolinium nitrate and citric acid. The Mg and Mg-Mn ferrites were prepared by using two different methods namely citrate precursor method (CPM) and solution combustion method (SCM). The detail experimental process related to this research work is enunciated and various characterization methods are explained in this chapter.

Chapter four describes the results and discussion, which has been divided into five sections, where Section I describes about the optimization of synthesis method to produce $MgFe_2O_4$ ferrite. Section II explains about the effect of Fe deficient on the electromagnetic properties of Mg-Mn ferrites, Section III presents about the effect of

Tm substitution on electromagnetic properties of Mg-Mn ferrite, Section IV narrates about the effect of Gd substitution on structural and electromagnetic properties of Mg-Mn ferrite and finally Section V deals with the antenna application of the final product (Mg-Mn ferrite).

Chapter five contains the conclusions of this research work and the scope of the future work.

CHAPTER 2

LITERATURE REVIEW

2.1 Introduction

Ferrites are debuted as an important new category of magnetic materials and have been created since the last 50 years. The use of magnetic materials to perform vital functions is not limited to the utility industry, other industries consuming appreciable amounts of magnetic materials include communications, computer, audio-visual, and home appliances. In spite of this development in the technology of ferrite materials, scientists still prefer to examine the structure and transport properties of these materials in a systematic manner to evolve correlations between them. Therefore, it is necessary to understand the theory of magnetism and the basic properties of ferrites pertaining to study the magnetic materials that are using in many applications in our life.

2.2 Crystal structure of ferrite

The crystal structure of a ferrite can be regarded as an interlocking network of positively-charged metal ions (Fe^{3+}, M^{2+}) and negatively-charged divalent oxygen ions (O^{2-}). The arrangement of the ions or the crystal structure of the ferrite plays an important role in determining the magnetic interactions and therefore, the magnetic properties [Goldman, 2006].

The ferrite has the general formula of MFe_2O_4 where M is a divalent ion. This ferrite crystallizes in the cubic spinel structure and it contains 8 formula units in one unit cell. The spinel lattice is composed of a close-packed oxygen arrangement in

which 32 oxygen ions form the unit cell (the smallest repeating unit in the crystal network). These anions are packed in a face centered cubic (fcc) arrangement leaving two kinds of spaces between anions: tetrahedrally coordinated sites (A), surrounded by four nearest oxygen atoms, and octahedrally coordinated sites (B), surrounded by six nearest neighbor oxygen atoms. These are illustrated in Figure 2.1. In total, there are 64 (8 x 8) tetrahedral sites and 32 (4 x 8) octahedral sites in the unit cell, of which only 8 tetrahedral sites and 16 octahedral sites are occupied, resulting in a structure that is electrically neutral [Spaldin, 2003].

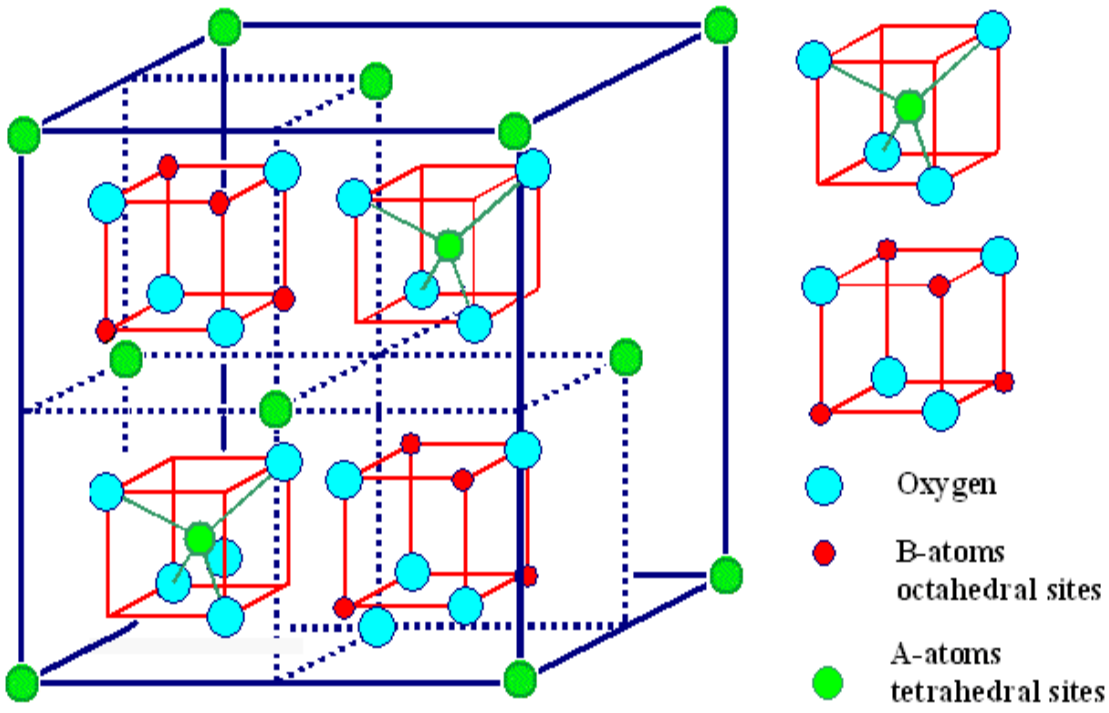

Figure 2.1: Two sub cells of a unit cell of the spinel structure
[Naseri and Saion, 2012]

The localization of ions either in the A or B sites depends fundamentally on the ion and lattice sizes. Also it has been observed to depend on the temperature and the orbital preference for specific coordination.

In general, divalent ions are larger than trivalent ions (Table 2.1). This is because trivalent ion nuclei produce greater electrostatic attraction, hence their electron orbits contract. The octahedral sites are larger than the tetrahedral sites, thus, the divalent ions are localized in the octahedral sites where as trivalent ions are in the tetrahedral sites [Goldman, 1990].

Table 2.1: Radii of metal ions involved in Spinel ferrite [Goldman, 2006]

Metal ion	Ionic radius (Å)
Mg^{2+}	0.78
Mn^{3+}	0.70
Mn^{2+}	0.91
Fe^{2+}	0.83
Fe^{3+}	0.67
Co^{2+}	0.82
Ni^{2+}	0.78
Cu^{2+}	0.70
Zn^{2+}	0.82
Cd^{2+}	1.03
Al^{3+}	0.57
Cr^{3+}	0.64

There are three different types of spinel structure have to be distinguished by considering the distribution of cations over the two possible sites (A site and B site).

(1) Normal spinel

(2) Inverse spinel

(3) Mixed spinel

In the normal spinel structure, the trivalent cations are found only on the B sites, while divalent cations occupy the A sites. For example, in the case of zinc ferrite, the tetrahedral-A sites are occupied by zinc ions, which being non-paramagnetic (having no unpaired electronic spin) produce no anti-ferromagnetic orientation of the ions on the octahedral-B sites that are occupied by Fe^{3+} ions. The Fe^{3+} (B-B) interactions are so weak as to be unimportant. Therefore, zinc ferrites present paramagnetic behavior. This type of arrangement is called a normal spinel structure. The ion distribution on the A-site and B-site is shown in Table 2.2.

On the other extreme, the inverse spinel structure, the divalent ions occupy only B-sites while trivalent ions are distributed on both A and B-sites in equal proportion. Considering the case of nickel ferrite, eight units of $NiFe_2O_4$ go into a unit cell of the spinel structure. The ferric ions preferentially fill the tetrahedral sites, but there is room for half of them (eight). The remaining go on the octahedral sites as do the eight Ni^{2+} ions. The antiferromagnetic interaction orients these eight Fe^{3+} moments and eight nickel moments antiparallel to the eight Fe^{3+} moments on the tetrahedral sites. The Fe^{3+} ions moments will just cancel, but the moments on the nickel ions give rise to an uncompensated moment or magnetization. This type of ferrite is called an inverse ferrite (Table 2.2).

The mixed spinel is a mixture between the normal and inverse spinel. It is possible to get different mixture of the two. For instance, in a Ni-Zn ferrite, 50% of the Nickel divalent magnetic ion (Ni^{2+}) is replaced with Zn^{2+}. The Zn^{2+} goes on to half of the tetrahedral (A) sites and the other half of the A sites for Fe^{3+} ions. The remaining Fe^{3+} ions go to the octahedral (B) sites. On the tetrahedral sites, the Fe^{3+} moments are orient all the octahedral site moments antiparallel to them. Therefore the Fe^{3+} moments on the tetrahedral sites neutralize only one third of the octahedral Fe^{3+} ions that leave a large percentage (i.e the other two thirds) oriented, but uncompensated giving a net magnetic moment.

Table 2.2: Metal ion distribution in ferrites. [Baltzer, 1965]

	Metal ions on lattice site				
	A (tetrahedral sites)		B (Octhedral sites)		Resultant
Type of ferrites	Ions	Moment	Ions	Moment	Moment
Zinc Ferrite (Normal Spinel)	Zn^{2+}	___	Fe^{2+}	↓ ↑	0
Nickel Ferrite (Inverse Spinel)	Fe^{3+}	↓	Fe^{3+} Ni^{2+}	↑ ↑	↑
Nickel-Zinc Ferrite (Mixed Spinel)	Fe^{3+} Zn^{2+}	↓	Fe^{3+} Ni^{2+}	↑ ↑	↑

2.3 Crystal structure of orthoferrite

Rare earth orthoferrites are classified as ferrites. The magnetic oxides with perovskite structure are an exception in the group of oxides. The perovskite structure is shown schematically in Figure 2.2. Large divalent or trivalent ions (A) occupy the corners of a cube and small trivalent or tetravalent metal ions (B) occupy the centre of the cube. The oxygen ions are situated centrally on the faces of the cube. The general chemical formula is ABO_3, where A represents a rare earth.

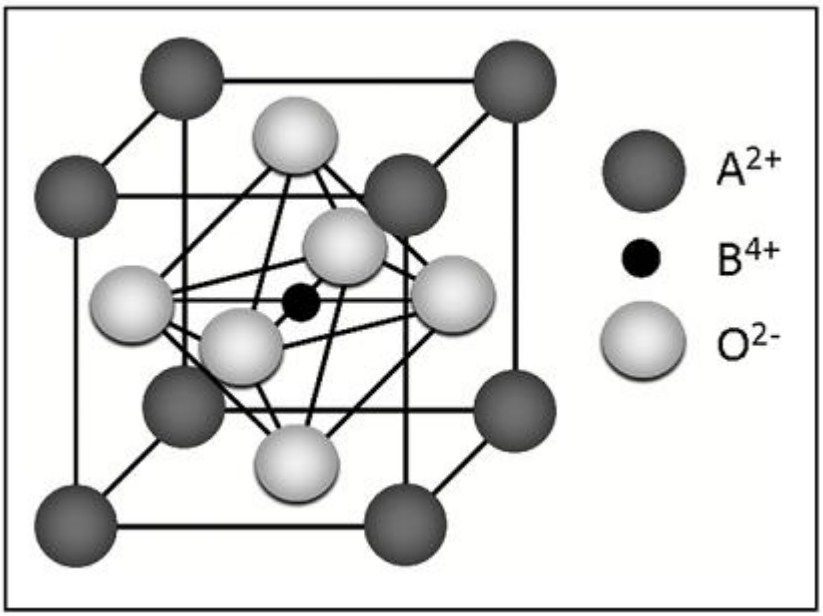

Figure 2.2: A Perovskite structure of an orthoferrite [Schmool, et al, 1999]

The magnetic structure inside of a sublattice is usually collinear ferromagnetic, but the different sublattices are coupled antiferromagnetically. Due to the different number of magnetic ions in different sublattice, there is a net resulting magnetic moment, giving rise to ferrimagnetism. The nature of the superexchange interaction depends not only on the type of the magnetic ion, but rather strongly on

the bond length and bonding angle. This makes it possible to change the strength and type of the superexchange interaction.

2.4 Magnetic properties

Understanding of magnetism cannot be attained clearly without a sound knowledge of the way in which magnetic properties are measured. Magnetism is a phenomenon by which the materials assert an attractive or repulsive or influence of other materials, has been known for thousands of year. The basic principles and mechanism that explain the magnetic phenomenon are complicated and understanding of their properties has eluded scientists until relatively recent times.

2.4.1 Basic concepts

2.4.1.1 Magnetic Field and Dipoles

A magnetic field is a field of force produced by moving electric charges, by electric fields that vary in time and by the intrinsic magnetic field of elementary particles associated with the spin of the particle. It is convenient to understand the magnetic forces in terms of fields. Magnetic dipoles are found to exist in magnetic materials. Magnetic dipole occurs in pairs and composed of north and south poles instead of negative and positive electric charges. The force of the field itself exerts a torque within a magnetic field that tends to orient the dipoles with the field [Callister, 2007].

2.4.1.2 Origin of Magnetic moments

The origin of magnetism was explained by Goudsmit and Uglenbeck by introducing the concept of electron spin in 1925 and 1926 [Goldman, 2006]. Each

electron in an atom has magnetic moments that originate from two sources. One source involves the orbital motion of electrons around the nucleus; being a moving charge, an electron may be considered as a small current loop that generate a very small magnetic field, and having a magnetic moment along its axis of rotation. It is schematically illustrated in Figure 2.3 (a). Another source of magnetic moment originates from the electron spin which corresponds to the movement of electric charge in electron, hence an electric current that produces a magnetic moment in the atom (Figure 2.3 – b). The amount of net magnetic moment of an atom is the vector sum of the individual spin and orbital moments of the electrons in its outer shells.

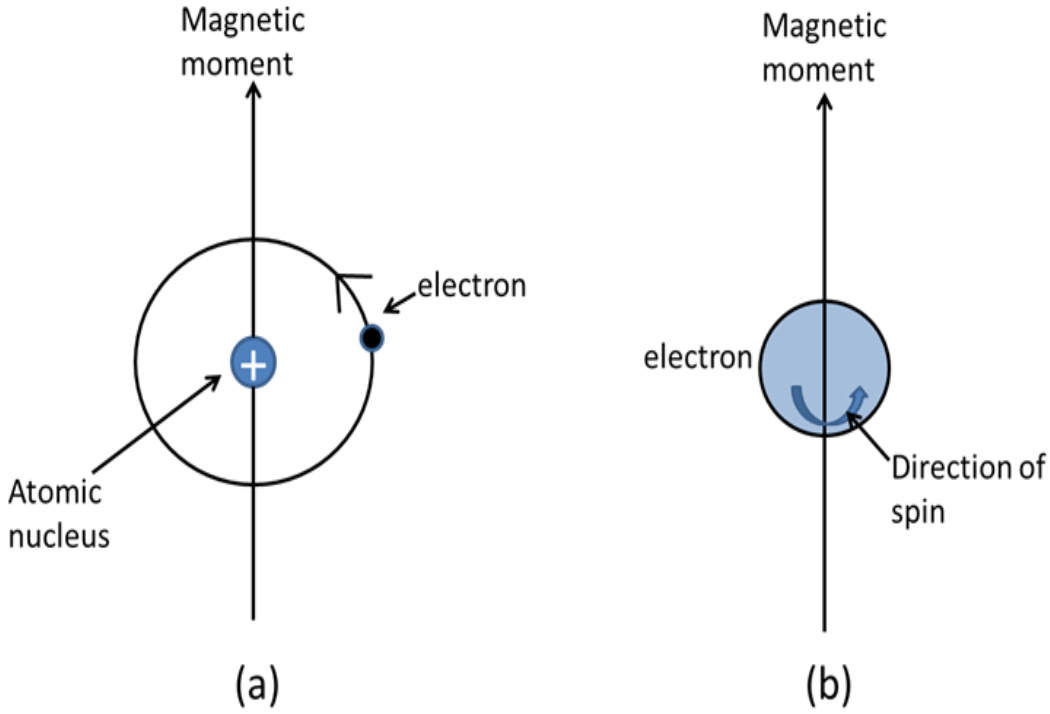

Figure 2.3: Demonstration of the magnet moment associated with (a) an orbiting electron and (b) a spinning electron [Callister, 2007].

There are two types of electron spin which are commonly represented as arrows pointed up or down. Each electron in an atom may be considered as being a small magnet having permanent orbital and spin magnetic moments. The Bohr

magneton μ_B is the most fundamental magnetic moment and Table 2.3 shows the number of Bohr magnetons for some ions.

Table 2.3: Bohr magneton of ions commonly found in magnetic materials [Goldman, 2006]

Ion	Bohr Magneton (μ_B - J/T^{-1})
Fe^{2+}	4
Fe^{3+}	5
Co^{2+}	3
Ni^{2+}	2
Mn^{2+}	5
Mg^{2+}	0
Zn^{2+}	0
Li^{2+}	0

2.4.1.3 Magnetic behavior

Magnetic materials are classified by their response to an externally applied magnetic field. Different kinds of magnetism observed in nature can be identified by the help of the descriptions of orientations of magnetic moments in a material (Figure 2.4).

The main types of magnetism are following: diamagnetism, paramagnetism, antiferromagnetism, ferromagnetism and ferrimagnetism. When a magnetic field is applied to a substance the electron motions are modified and a small net magnetization is induced in a sense opposing the applied field as well as it will create the atomic current loops. All materials display this type of weak repulsion to a magnetic field known as diamagnetism. It is very weak form of magnetism and has

very small negative susceptibilities (about 10^{-6}). The effects of these atomic current loops are overcome if the material has long–range ordering of magnetic moments [Chen, 1986].

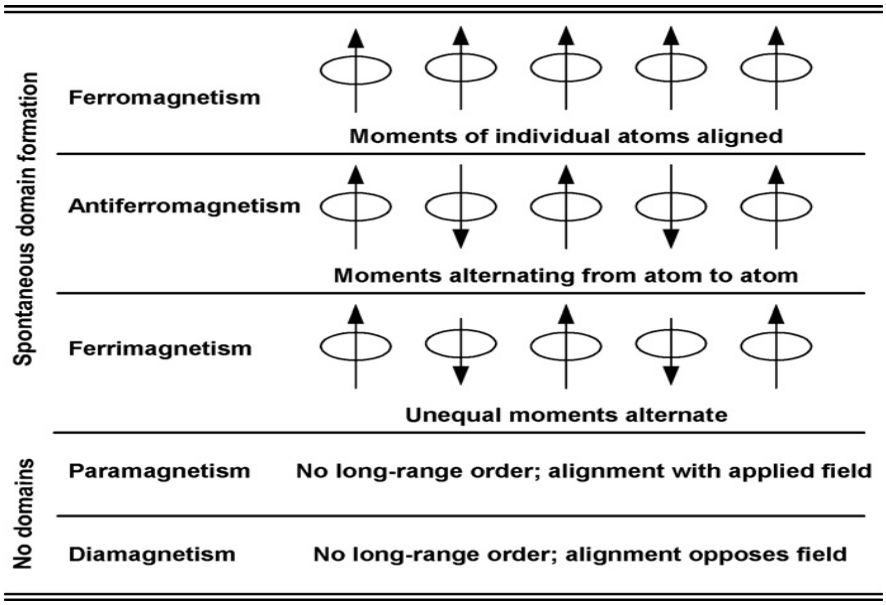

Figure 2.4: Different types of magnetic behavior [Mathew, 2007]

For some solid materials, each atom has a permanent magnetic moment arising from the spinning and orbiting electrons. The orientations of these atomic magnetic moments are random in the absence of an external magnetic field. Hence, a piece of material possesses no net macroscopic magnetization. These magnetic moments are free to rotate in any direction and when they preferentially align, by rotation with an external field, this is called paramagnetism. Thus, paramagnetic materials moments have no long-range order and there is a small positive magnetic susceptibility ($\chi \approx 0$), in the range of 10^{-3} - 10^{-6} [Moulson and Herbert, 1992].

In ferromagnetic materials, a parallel arrangement of magnetic moments in neighbouring atoms and in the same direction giving rise to a high value of magnetic

moments. These materials are spontaneously magnetized below a temperature termed the Curie temperature. Therefore, below this temperature, the aligned moments in ferromagnetic materials can confer a spontaneous magnetization in the absence of an applied magnetic field [O'Handley, 2000]. Hard or permanent magnets display ferromagnetism in the absence of an external field. The magnetic moment coupling results in an antiparallel alignment meaning that the alignment of the spin moments of neighboring atoms or ions in exactly opposite directions is termed antiferromagnetism [Tilley, 2004]. There is a zero net magnetization when the spins oriented in antiparallel to opposite directions in the absence of magnetic field.

Ferrimagnetism characterizes a material which is microscopically like antiferromagnetic. But in which the magnetization of the two sublattices are not the same. There is no more compensating each other exactly in the two sublattices. So that, a resultant uncompensated magnetic moment from the unpaired spin always exists in ferrimagnetic materials. Ferrites exhibit ferrimagnetic behavior [Cullity and Graham, 2009].

2.4.1.4 Magnetic domain

A magnetic domain describes a region within a magnetic material which has uniform magnetization [Hubert and Schafer, 2009]. This means that the individual magnetic moments of the atoms are aligned with one another and they point in the same direction as illustrated in Figure 2.5. When heated above a temperature called the Curie temperature, a piece of ferromagnetic material undergoes a phase transition, and the uniform magnetization within a domain spontaneously disappears: each atom has its own direction of magnetic moment, independent from its

neighbouring atoms. Magnetic domain structure is responsible for the magnetic behavior of ferromagnetic materials like iron, nickel, cobalt and their alloys, ferrites etc. Domains contain about 10^{12} to 10^{15} atoms and the regions separating magnetic domains are called domain walls (Figure 2.6) [Spaldin, 2003], where the magnetization rotates coherently from the direction in one domain to that in the next domain.

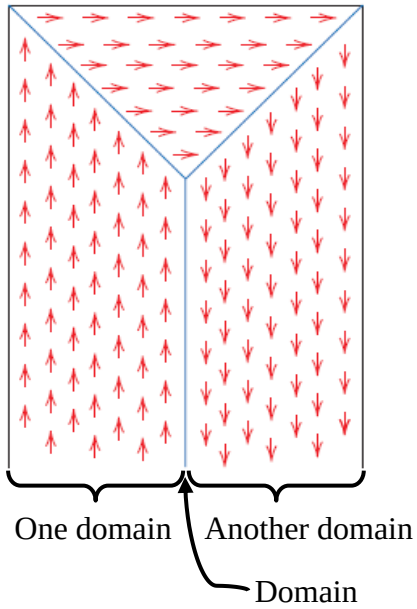

Figure 2.5: Schematic depiction of domains in a ferromagnetic or ferrimagnetic material

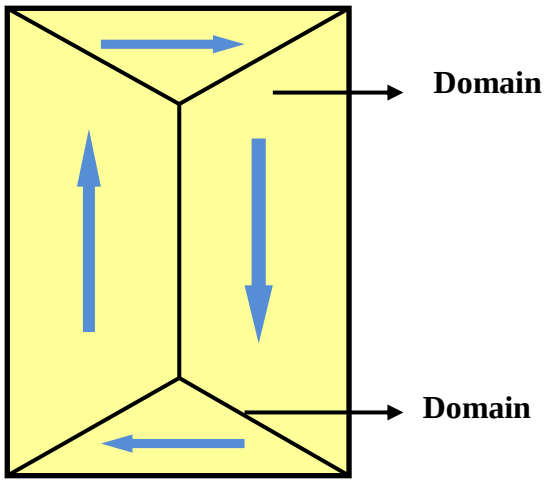

Figure 2.6: Illustration of Domain and Domain Wall

If consider a large single crystal of a uniaxial substance is entirely one domain, it is spontaneously magnetized parallel to the easy axis, as in Figure 2.7 (a). Then free poles form on the ends and these poles are the source of a large magnetic field, H [Cullity, 1972]. The magnetostatic energy of this crystal is evaluated over all space where H is appreciable. This considerable energy can be approximately halved, if the crystal splits into two domains magnetized in opposite directions as in Figure 2.7 (b), because this brings north and south poles closer to one another, thus decreasing the spatial extent of the H field. If the crystal splits into four domains as in Figure 2.7 (c), the magnetostatic energy again decreases, to about one-fourth of its original value. This splitting process continues to lower the energy of the system until the point that more energy is required to form the domain boundary than is decreased by the magnetostatic energy change.

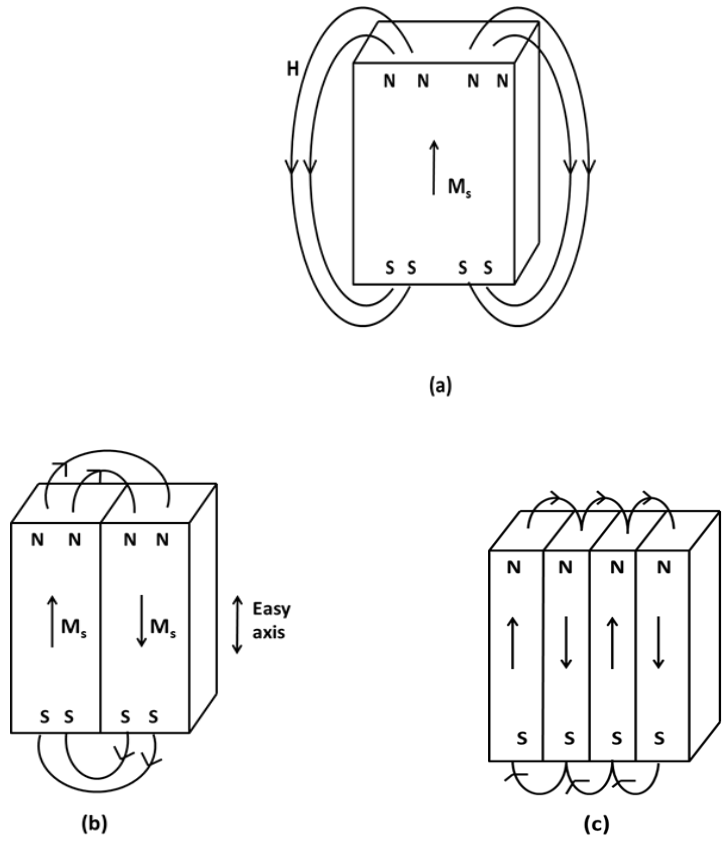

Figure 2.7: Division into domains [Rabe et al., 2007].

The net magnetization of all domains in a specimen is zero in the absence of an applied field. When an H field is applied, the domains change shape and size by the movement of domain boundaries. Initially, the movements of the constituent domains are randomly oriented such that there is no net magnetic field. As the external field is applied, the domains that are oriented in directions favorable to the applied field grow at the expense of those that are unfavorably oriented. This process continues increasing field strength until the macroscopic specimen becomes a single domain, which is nearly aligned with the field. Saturation magnetization is achieved when this domain, by means of rotation, becomes oriented with the magnetic field [Weiss, 1971].

2.4.1.5 Metal ions distribution over octahedral and tetrahedral sites

The distribution of the Fe and divalent metal ions between the octahedral and tetrahedral sites of the spinel lattice is governed on the interesting and useful electromagnetic properties of the spinel ferrites [Wei et al., 2001]. Hence, the knowledge of cation distribution is essential to understand the magnetic system of ferrites. In general, possible cation distributions can be observed and represented by [Ziolkowski et al., 1996]:

$$\left(Me_{\gamma}^{2+}Fe_{1-\gamma}^{3+}\right)\left[Me_{1-\gamma}^{2+}Fe_{1+\gamma}^{3+}\right]O_4$$

where the cations in parentheses are on A- tetrahedral sites and those in the square brackets are on B- octahedral sites. The parameter Me represents the metal ion and γ is the degree of inversion (i.e., fraction of Fe^{3+} on A sites). The limiting case of $\gamma = 0$ corresponds to the normal spinel structure; $\gamma = 1$ corresponds to the inverse spinel

structure; and $\gamma = 2/3$ corresponds to random distribution of cations [Willard et al, 1999]. The occupation of cations in the different magnetic sublattices would be affected by the preparation methods and heat treatment, leading to changes in the magnetic properties. Singh, (2006) was proved and reported that Mg-Mn ferrite is a mixed spinel and the cation distribution can be varied by the different preparation techniques.

2.4.1.6 Magnetic interactions in ferrites

In ferrites, Neel (1948) assumed that a ferromagnetic crystal lattice could be divided into two sublattices such as would be formed by the A (tetrahedral) and B (Octahedral) sites in a spinel structure. Also he postulated that magnetic moments of ferrites are the sum of magnetic moments of individual sublattices. There are three possible interactions between magnetic ions to be considered and these may be classed as

(1) A-A interactions

(2) B-B interactions and

(c) A-B interactions.

With regard to the strength of interactions between moments on the various sites, the negative interaction between the moments of two metal ions on different sites depends on the distances between these ions and the oxygen ions (p, q, r, s) and also on the angle between the three ions (α). The distance and angle between the metals and oxygen atoms in the spinel structure are given in Figure 2.8. The exchange energy is greatest for an angle of 180^{o} and also where the interatomic distances are the shortest. In the A-A and B-B interactions, the angles are too small